IOP Publishing Journal of Physics D: Applied Physics

J. Phys. D: Appl. Phys. **51** (2018) 155201 (8pp) https://doi.org/10.1088/1361-6463/aab322

Consequences of atomic layer etching on wafer scale uniformity in inductively coupled plasmas

Chad M Huard[1], Steven J Lanham[2] and Mark J Kushner[1,3]

[1] Department of Electrical Engineering and Computer Science, University of Michigan, 1301 Beal Ave., Ann Arbor, MI 48109-2122, United States of America
[2] Department of Chemical Engineering, University of Michigan, 2300 Hayward St., Ann Arbor, MI 48109-2136, United States of America

E-mail: chuard@umich.edu, sjlanham@umich.edu and mjkush@umich.edu

Received 29 December 2017, revised 3 February 2018
Accepted for publication 1 March 2018
Published 19 March 2018

Abstract

Atomic layer etching (ALE) typically divides the etching process into two self-limited reactions. One reaction passivates a single layer of material while the second preferentially removes the passivated layer. As such, under ideal conditions the wafer scale uniformity of ALE should be independent of the uniformity of the reactant fluxes onto the wafers, provided all surface reactions are saturated. The passivation and etch steps should individually asymptotically saturate after a characteristic fluence of reactants has been delivered to each site. In this paper, results from a computational investigation are discussed regarding the uniformity of ALE of Si in Cl_2 containing inductively coupled plasmas when the reactant fluxes are both non-uniform and non-ideal. In the parameter space investigated for inductively coupled plasmas, the local etch rate for continuous processing was proportional to the ion flux. When operated with saturated conditions (that is, both ALE steps are allowed to self-terminate), the ALE process is less sensitive to non-uniformities in the incoming ion flux than continuous etching. Operating ALE in a sub-saturation regime resulted in less uniform etching. It was also found that ALE processing with saturated steps requires a larger total ion fluence than continuous etching to achieve the same etch depth. This condition may result in increased resist erosion and/or damage to stopping layers using ALE. While these results demonstrate that ALE provides increased etch depth uniformity, they do not show an improved critical dimension uniformity in all cases. These possible limitations to ALE processing, as well as increased processing time, will be part of the process optimization that includes the benefits of atomic resolution and improved uniformity.

Keywords: plasma etching, atomic layer etching, inductivley coupled plasmas

(Some figures may appear in colour only in the online journal)

1. Introduction

The wafer scale uniformity of plasma etching processes is critically important to semiconductor fabrication [1]. Techniques to address the uniformity of plasma properties, and in particular the uniformity of reactant fluxes to etching surfaces, continue to be a high priority [2–4]. As feature sizes and film thicknesses shrink, conventional techniques to obtain uniform reactant fluxes and etch rates are being challenged to meet process demands. Techniques to locally adjust continuous etch rates to accommodate plasma non-uniformities have been studied, but typically require increased tool complexity [5,6]. Atomic layer etching (ALE) processes, which rely on self-limited reactions, are less sensitive to the uniformity of reactant fluxes and may increase the wafer scale etching uniformity in many applications.

[3] Author to whom correspondence should be addressed.

Plasma based ALE is a self-limiting two-step process capable of removing single atomic layers in each cycle [7]. The first step of the cycle passivates the surface in a manner that naturally stops when the top surface layer is fully passivated. This step is ideally performed with an ion-free flux of neutral radicals. In the second step, the passivated layer is selectively removed by, ideally, a radical free flux of energy-controlled ions that chemically sputters the top passivated layer but is not energetic enough to sputter the underlying unpassivated atoms. When the fluence of reactants is large enough to fully saturate both of the self-limited half-reactions, the etch depth per cycle (EPC) should be constant. In this saturated regime, the etch rate should also be independent of small non-uniformities in the reactant fluxes. The adoption of ALE techniques may then offer a way to obtain atomic scale uniformity over large areas without the need for having correspondingly uniform reactant fluxes.

Although ALE of several materials has been demonstrated [8–10], silicon is often used as the test case to demonstrate ALE principles as its passivation and etch steps are perhaps the most clear. In the ALE of silicon, chlorine containing plasmas are often used for the passivation step. Following passivation of the silicon surface, a rare gas plasma, often argon, is used for the removal step [11]. In the passivation phase, Cl radicals passivate Si sites to form $SiCl_x$ ($x \leqslant 3$). This process is inherently self-limited due to the strength of the Si–Cl bond, and the low solubility and diffusivity of Cl into the bulk silicon. The removal of passivated silicon by ion bombardment can be made self-limited by controlling ion energies to be above the sputtering threshold of $SiCl_x$ and below that of bare Si [12].

Self-limiting behavior is necessary to improve wafer scale uniformity in the presence of non-uniform reactant fluxes, but it is not clear what the relationship is between the uniformity enabled by ALE and process saturation. Most ALE processes are not perfectly self-limited [13], and it is difficult to estimate the effect of non-ideal etching reactions on process uniformity. The following discussion focuses on the consequences of saturation during the ion bombardment phase of ALE on wafer-scale uniformity, however the same trends hold true for the passivation phase as well.

Assuming a Langmuir kinetic model for the desorption of passivated surface sites during ion bombardment, and perfect self-limited behavior, the EPC at radius r on the wafer of an ALE process can be estimated as

$$\mathrm{EPC}\,(r) \sim 1 - \mathrm{e}^{-\Gamma_\mathrm{i}(r)T_\mathrm{i}/\Phi_\mathrm{c}}\ \ (\mathrm{ML/cycle}), \tag{1}$$

where $\Gamma_\mathrm{i}(r)$ is the ion flux at radius r, T_i is the ion bombardment time and Φ_c is the ion fluence characterizing the saturation behavior. The units of EPC, ML/cycle, are monolayers of material per ALE cycle. To obtain uniform etch rates when ion fluxes to the wafer are not uniform, the smallest ion fluence onto the wafer must be large compared to Φ_c,

$$\Phi_\mathrm{i}\,(r) = \Gamma_\mathrm{i}(r)T_\mathrm{i} \gg \Phi_\mathrm{c}. \tag{2}$$

This relationship specifies the minimum value of T_i that will produce saturated ALE behavior across the entire wafer.

In this paper, results are discussed from a computational investigation of the wafer-scale uniformity of ALE in inductively coupled plasmas (ICPs) sustained in Ar/Cl_2 mixtures when the reactant fluxes are non-uniform. It was found that ALE can reduce the sensitivity of the etch rate to the uniformity of the incident ion flux, even when the process is not fully self-limited (non-ideal ALE). The sensitivity of etch uniformity to the uniformity of the ion flux increases when the ALE process is operated in the sub-saturation regime, but remains sub-linear. Finally, the ALE process was found to expose the surface to a higher ion fluence than continuous etching for a given etch depth. The models used in this investigation are briefly described in section 2, followed by our discussion of ALE enabled uniformity in section 3. Our concluding remarks are in section 4.

2. Description of the models

The reactor scale plasma model [14], feature scale model [15] and surface reaction mechanism [16] used in this investigation have been described previously, and so are only briefly discussed here.

Modeling of reactor scale conditions for the ICPs was performed using the hybrid plasma equipment model (HPEM) [14]. The HPEM solves Maxwell's equations to produce the varying electromagnetic fields in the reactor due to the antenna current. These fields are then used to produce the spatially dependent electron energy distribution (EED) by solving the Boltzmann equation using Monte Carlo techniques in the presence of energy dependent electron impact collisions. Source and loss terms due to electron impact collisions are calculated from the EEDs, and passed to the fluid kinetic model (FKM), which solves continuity, momentum and energy equations separately for ion and neutral gas species. Poisson's equation for the electrostatic potential is solved in the FKM using the position dependent charge density in the gas phase and on surfaces. Each of these processes is iteratively repeated until a converged solution is produced. Each module uses a different timescale to match the characteristic timescale of the physical process being addressed, with the results being combined using a hybrid time slicing technique to speed conversion to the plasma steady state. Once plasma conditions converge to a steady state, ion energy and angular distributions (IEADs) to the wafer are calculated using Monte Carlo techniques to track ion trajectories from the bulk plasma through the sheath, including collisions along the path.

The surface plasma interaction on the wafer was modeled using the 3D Monte Carlo feature profile model (MCFPM) [15]. The MCFPM divides the feature simulation domain into cubic voxels, with each cell representing a single material. These materials may be elemental, or compounds (e.g. Si, SiCl, $SiCl_2$). Gas phase pseudoparticles are generated with statistical distributions using Monte Carlo techniques based on reactive species fluxes to the wafer obtained from the FKM, and IEADs from the HPEM. Particles are propagated through the simulation domain until they interact with solid material cells. When a collision is detected between a gas phase pseudoparticle and a solid material cell, a reaction for that gas/solid pair is chosen from a user defined reaction mechanism. These

reactions can include chemical reactions (which change the material identity of the cell), etching reactions (which convert the impacted cell to a gas cell), deposition reactions (which deposit a new solid cell on top of the impacted cell) or a reflection of the incoming particle without reaction. The probabilities of these reactions can be dependent on the energy and incident angle of the incoming particle (sputtering reactions) or have fixed probabilities (thermal reactions).

The reaction mechanism used here for Ar/Cl_2 plasma etching silicon is dominated by chemical etching of chlorinated silicon [16]. Chlorination of the bare silicon proceeds sequentially—from bare silicon to SiCl, $SiCl_2$ and finally $SiCl_3$—by exposure to chlorine radicals. The probability of chlorine uptake drops with increasing chlorination. The probability of an energetic particle sputtering a chlorinated $SiCl_x$ cell increases with particle energy and chlorination level. Direct sputtering of bare, un-chlorinated silicon (physical sputtering) is included with a larger energy threshold and lower probability than chemical sputtering of chlorinated silicon. Thermal etching of $SiCl_3$ sites by chlorine radicals is also included with a low probability. Both thermal etching and physical sputtering of silicon contribute little to the etch process during continuous etching, but can become important during ALE. The feature scale model and surface reaction mechanism were modified from the model previously described to account for ion penetration into the silicon, and the resulting mixing. This effect was not found to be important to the results presented here and will not be discussed further.

3. Scaling of ALE with uniformity of fluxes

The plasma etching reactor used for this study was 53.4 cm in diameter, with a 3 turn radio frequency (RF) antenna located behind a quartz window 9.5 cm above the 30 cm diameter wafer. The radial position of this antenna was varied to produce three patterns of ion flux onto the wafer. Antenna A1 is located close to the edge of the reactor, A2 is centered in the reactor radius and A3 is close to the center of the reactor. The geometry, antenna configurations, and the resulting plasma density profiles are shown in figure 1. This reactor was intentionally given a somewhat wider aspect ratio and narrower antenna pattern than is typical for devices optimized for uniformity of reactant fluxes to the wafer. These configurations result in plasma non-uniformity which is exaggerated from best practice to clearly show the differences between continuous etching and ALE, as well as to explore the limits of how much flux non-uniformity ALE is capable of compensating for.

For each of the three antenna configurations, simulations were performed using an $Ar/Cl_2 = 90/10$ mixture (for continuous etching), a pure Cl_2 mixture (for ALE passivation) and Ar contaminated with 10 ppm of Cl_2 (for ALE ion bombardment). The antenna was powered at 10 MHz, the RF bias on the substrate was 10 MHz and gas flow rate was 600 sccm held at a pressure of 10 mTorr using a feedback controlled gate valve. The wafer was divided into five regions—evenly spaced in radius—and statistics for the distribution of ion energies

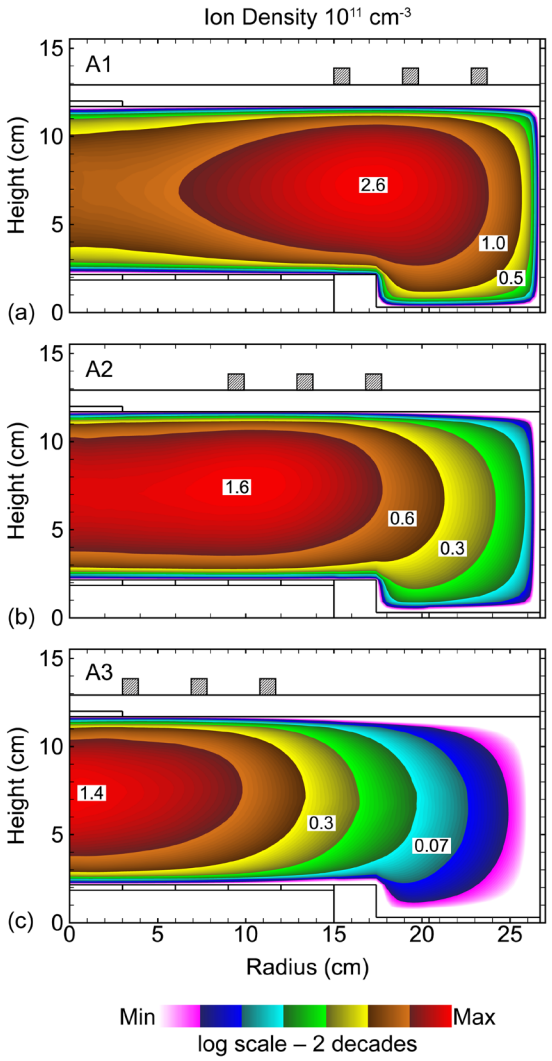

Figure 1. Reactor geometry and total ion density for three different antenna configurations. Antennas, from top to bottom are: (a) A1, (b) A2 and (c) A3. The ion densities are for the argon plasma used in ion bombardment during ALE—$Ar/Cl_2 = 100/10$ ppm, 10 mTorr. Powers were adjusted to provide the same ion flux to the center of the wafer.

and incident angles were separately collected for each region. Combined with fluxes of each reactant species (Ar^+, Cl^+, Cl_2^+ and Cl), a piecewise assessment of the consequences of non-uniformity in reactant fluxes, ion energies and angular distributions can be taken into account in the etching model.

The introduction of 10 ppm Cl_2 contamination in the argon feedstock gas during the ion bombardment phase of ALE is intended to represent the residual chlorine in the system from incomplete purging of the gas lines, adsorption of Cl on the reactor walls or dissociation of Cl containing etch products by electron impact. The results of simulating the Cl_2 contaminated argon plasma indicate a finite ion-to-neutral ratio ($90 < \Gamma_i/\Gamma_n < 650$) during the ion bombardment phase. The Γ_i/Γ_n ratio changes with both position on the wafer and antenna configuration. The presence of chlorine during the ion bombardment phase introduces an etching reaction which is not fully self-limited. The high energy tails of the ion energy distribution also extend slightly beyond the 50 eV

threshold set for physical sputtering of the underlying silicon, which introduces another continuous, non-self limited etching pathway during the ion bombardment phase. These combined pathways result in the amount of material removed in the ion bombardment phase not being fully self-limited and therefore dependent on the ion bombardment step time (T_i).

The ion fluxes to the wafer as a function of radius are shown in figure 2 for the three antenna configurations. The same radial dependence occurs for both continuous etching using the $Ar/Cl_2 = 90/10$ mixture, and during the ion bombardment phase of ALE using the Ar with Cl_2 contamination. Using antenna A1 results in an ion flux which increases from the center of the wafer to the edge. The ion flux generated by antenna A2 has a local minimum at the center of the wafer with a local maximum at a radius of ≈10 cm. Antenna A3 has a maximum in ion flux at the center of the wafer, decreasing monotonically with increasing radius.

In addition to the non-uniform ion flux, using constant ICP power for each antenna configuration results in there being different magnitudes of fluxes to the wafer between antennas. To make comparisons between the antennas, the power was scaled roughly with the radiating area of each antenna, which approximately matches the power per unit volume, and results in a similar ion flux at the center of the wafer for each antenna. The powers were 600 W for antenna A1, 300 W for A2 and 111 W for A3. The different plasma density profiles generated by each antenna also produced a different dc bias on the substrate. As a result, the average ion energy reaching the wafer was different for each antenna even with the same RF bias amplitude applied to the substrate. To compensate and ensure that the average ion energy incident onto the wafer was consistent from antenna to antenna, the RF bias was adjusted such that the average ion energy at the center of the wafer was 30 eV. The same ICP power and RF bias voltage was used for both gas mixtures.

The reactor scale model also predicts non-uniformity in several plasma properties, other than ion flux, which are relevant to etching. The ion energy distribution (IED), particularly the maximum energy, varies with position on the wafer. This dependence of peak ion energy as a function of radius is caused by the variation in sheath width interacting with the finite transit time of ions accelerating through the sheath. Radii having lower plasma density resulted in a wider sheath at the surface of the wafer requiring a longer ion transit time. The longer transit time averages the ion trajectory over a larger portion of the 10 MHz cycle thereby reducing peak energy. The ratio of the flux of ions to reactive neutrals can also depend on antenna configuration and radial position. Since Cl radicals are produced by electron impact dissociation reactions, the non-uniformity of ICP power deposition results in a non-uniform radical flux, particularly in Cl_2 lean conditions. These non-uniformities in Cl radical flux and IEDs were included in modeling of etch rates, however they were found to be of secondary importance.

The pure Cl_2 plasma was used only for passivation of Si sites in this study, and so the conditions for the passivation step were selected separately from those for the Ar/Cl_2 plasmas to optimize the passivation process. The Cl_2 plasma

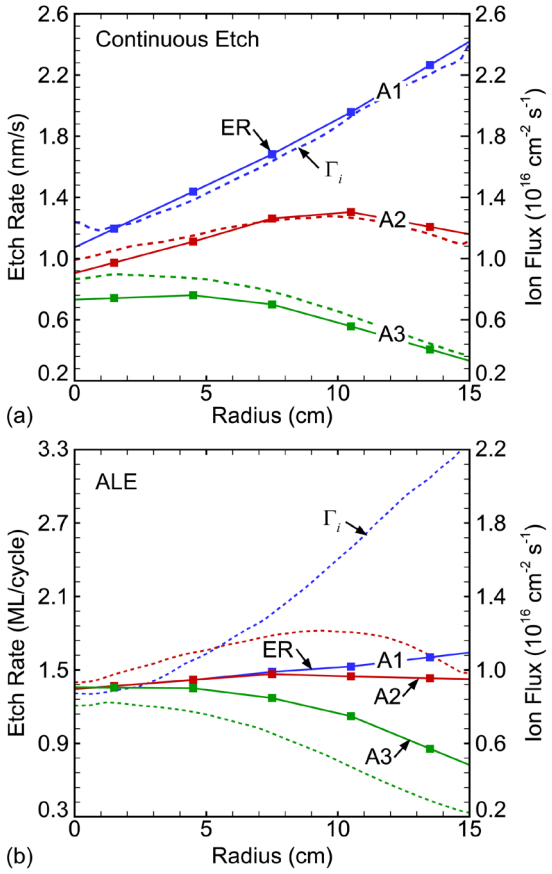

Figure 2. Etch rate and ion flux to the wafer as a function radius for three antennas, A1, A2 and A3. (a) Continuous etching ($Ar/Cl_2 = 90/10$) with etch rate in nm s^{-1}. (b) Ion fluxes from argon plasma with 10 ppm Cl_2 contamination with ALE rate in ML/cycle.

was sustained using 300 W of ICP power at 10 MHz, with no RF bias applied to the wafer. The resulting plasma conditions have a high neutral to ion ratio ($\Gamma_n/\Gamma_i = 300$–1200), and ion energies which were lower than the lowest sputtering threshold in the surface reaction mechanism. The fluxes of Cl radicals were fairly uniform for all conditions, resulting in little difference in passivation rates and outcomes between different antenna configurations.

To establish a baseline for comparing to ALE processing, continuous etching was simulated using the $Ar/Cl_2 = 90/10$ gas mixture. Continuous etching of blanket (un-patterned) silicon was simulated for each of five radial positions on the wafer using each of the three antenna configurations. The position dependent etch rates, shown as solid lines in figure 2(a), are nearly directly proportional to the total ion flux, indicating etching is operating in the ion-starved regime [17]. Etch rates for antenna A1 increase by 89% across the wafer, marginally more than the increase in in the ion flux, Γ_i (82%). The more rapid increase in etch rate compared to Γ_i is due to an increase in ion energy at the edge of the wafer where the sheath is thinner. The etch rates for antennas A2 and A3 also scale nearly linearly with ion flux. This linear dependence on Γ_i indicates that non-uniformities in other etch factors, such as IED and radical flux, are of secondary importance for these conditions, as appropriate in the ion-starved regime.

Atomic layer etching was modeled for the same reactor by cycling between exposure to the fluxes produced by the Cl_2 plasma without a bias to passivate the surface with Cl radicals, and to the Ar plasma with an RF bias providing moderately energetic ion bombardment to etch the passivated surface. Since the Cl_2 plasma used for passivation was in direct contact with the wafer, some non-ideal flux of ions was incident onto the wafer during passivation. This resulted in a small amount of continuous etching, but the dominant radical flux was essentially uniform. For this reason, the focus of this investigation will be limited to the effect of non-uniformity of the ion flux during the ion bombardment phase. For all cases, the passivation time was constant at 45 ms, which was long enough to fully saturate the silicon surface with chlorine.

The ion fluxes during the ion bombardment phase of the ALE cases are shown as a dotted line in figure 2(b) for each antenna. The radial dependence of the ion fluxes are similar to the continuous etching case, but with larger non-uniformities than in the Cl_2 plasma. With antenna A1 there is an increase of 130% in ion flux from the center of the wafer to the edge.

ALE using an ion bombardment time of 3 s produced significantly more uniform etch rates than continuous etching, with only a small positive correlation between etch rate and ion flux, as shown in figure 2(b). For antenna A1, the etch rate—measured here in monolayers of computational cells (3 Å) per cycle—increased by 17% from the center of the wafer to the edge, significantly less than the increase in Γ_i (133%). This improvement in etch uniformity compared to Γ_i indicates a fully saturated self-limited ALE reaction. Non-ideal continuous etching mechanisms result in some dependence of etch rate on Γ_i, and produce the remaining non-uniformity in etch rate.

While the ALE process significantly improved the etch rate uniformity for antenna A1 and A2 when compared to continuous etching, the results for antenna A3 are less improved. This result indicates that the ion fluence at the center of the wafer, which is similar for each antenna, is only just large enough to saturate the ion bombardment reaction. For the A1 and A2 antennas, the ion flux and fluence increase with radius. Given that both the passivation and ion phases are both fully saturated, the increasing fluence at larger radius does not produce a significantly higher etch rate. However, in the case of antenna A3, the ion fluence drops below saturation as the radius increases, causing the etch rate to depend more strongly on ion flux which decreases with radius.

The ICP power used for antenna A3 was chosen to result in similar ion flux at the center of the wafer as antennas A1 and A2. This choice of ion flux resulted in sub-saturation behavior at large radius where ion fluxes are the lowest when processed using the same ion bombardment time as A1 and A2. If the ion fluence was increased for case A3 so that the entire wafer was within the saturation regime, either by increasing the ICP power (resulting in a larger ion flux) or by increasing T_i, a similar increase in uniformity could be obtained for A3.

For plasma conditions which have been optimized for uniformity of the ion flux, the most effective way to change the ion fluence during ALE is to change the length of the ion bombardment phase, T_i. The ALE rates as a function of

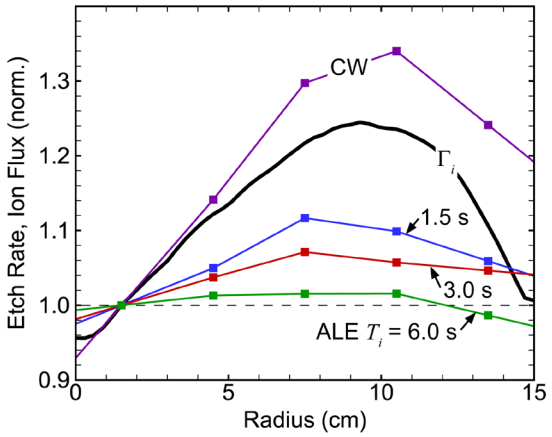

Figure 3. Etch rate and ion flux normalized to their values at a radius of 1.5 cm for different ion bombardment times (T_i = 1.5, 3.0 and 6.0 s) for antenna A2. 'CW' indicates the continuous etching rate.

radius for values of T_i from 1.5 s to 6 s are shown in figure 3 for antenna A2. The ion flux and rates for continuous etching are also shown for reference. The maximum ion flux is 20% larger than at the center and edge of the wafer. The etch rate with continuous etching (using the Ar/Cl_2 = 90/10 gas mixture) follows the radial trend of Γ_i, increasing by 30% from the center of the wafer to its maximum. The larger increase in etch rate compared to ion flux is due to radial non-uniformities in the ratio of ion to neutral fluxes, Γ_i/Γ_n, and ion energy.

All values of T_i produce ALE rates that are more uniform as a function of radius than the ion flux. The ALE rates become more uniform, and less sensitive to changes in ion flux, with increasing T_i. As saturation increases with increasing T_i, the dependence of etch rate on Γ_i decreases and the etch rate becomes more uniform. Since saturation has not been achieved in all cases, the EPC is different for each case at 1.5 cm radius. The EPC increases from 1.13 ML/cycle at T_i = 1.5 s to 1.37 ML/cycle at T_i = 3 s and 1.60 ML/cycle at T_i = 6 s. These differences in etch rate near the center of the wafer have been normalized out of the result in figure 3 to aid comparison between ALE cases, ion flux and continuous etch rates. Increasing T_i once full saturation has been achieved across the entire wafer (≈6 s) does not continue to improve etch rate uniformity, due to the presence of continuous etching mechanisms.

Completely saturated ideal self-limited reactions would result in an etch rate completely independent of the magnitude of the local ion flux, as implied by equation (1). This independence can be achieved using ideal ALE conditions (that is, no ions in the passivation phase and no radicals in the ion bombardment phase), as shown in figure 4. Here, ALE rates for each antenna and radial location for T_i = 1.5, 3 and 6 s are plotted as a function of ion fluence. For ideal ALE, once the critical ion fluence has been reached (≈10^{16} cm^{-2}), the etch rate (ML/cycle) is constant in spite of the significantly different conditions with different antennas. This trend reinforces the importance of ion flux non-uniformity (in the ion-starved regime) over other sources of non-uniformity in the model. Similar trends occur for non-ideal ALE, a saturation

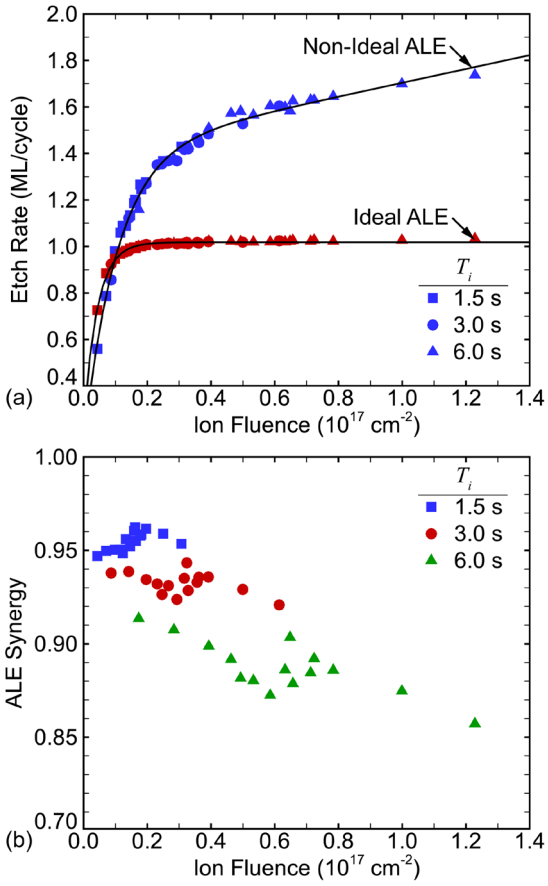

Figure 4. ALE rate and synergy as a function of ion fluence during a single ion bombardment sub-cycle. Data points from three ion bombardment times T_i are shown using different symbols (squares: $T_i = 1.5$ s; circles: $T_i = 3$ s; triangles: $T_i = 6$ s). For each T_i, data from all three antenna configurations is shown without differentiation. (a) Etch rate. (b) ALE synergy $\mathcal{S}_y$.

in the etch rate as the critical fluence is reached. However, for non-ideal ALE there is a finite positive slope in the etch rate as a function of ion fluence in the saturation region which results from continuous etching due to non-ideal reactions during ion bombardment. By removing the chlorine contamination from the ion bombardment phase, the ideal fluence-independent behavior in the saturation region is restored. This behavior is indicated by the horizontal line accurately fitting the etch rate of the ideal data for fluence greater than 0.3×10^{17} cm^{-2} in figure 4. In addition to providing an etch rate which is less dependent on ion fluence (in the saturation regime), ideal ALE reaches saturation at a lower ion fluence than performing ALE with non-ideal reactant fluxes. The larger characteristic fluence required to saturate the non-ideal ALE is due to the competition between the removal of passivated silicon by ion bombardment and the re-passivation of the underlying silicon by radical chlorine contamination.

The ALE synergy parameter ($\mathcal{S}_y$) is a measure of the ideality of the ALE process [13]. The $\mathcal{S}_y$ parameter is the total etch rate during an ALE process, minus the contributions from continuous etching, divided by the total rate. A value of $\mathcal{S}_y = 1.0$ indicates ideal, self-limited ALE while $\mathcal{S}_y = 0$ indicates etching in the absence of self-limited processes. Here, $\mathcal{S}_y$

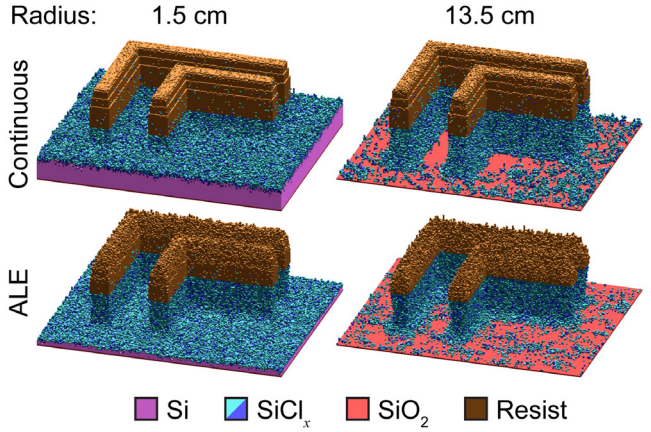

Figure 5. Predicted etch profiles for using antenna A1 for (top) continuous etching and (bottom) ALE at radii of (left) 1.5 cm and (right) 13.5 cm. $T_i = 3$ s for ALE cases. The two radial positions are etched for the same time, representing the non-uniformity on the wafer just before clearing the feature at the wafer edge.

was calculated by running three different simulations, one with only the ion bombardment conditions (no passivation phase), one with only the passivation conditions (no ion bombardment) and one for the complete cyclic ALE process. The tolerance of the ALE rate to non-uniformities in the ion flux is not directly related to $\mathcal{S}_y$. With there being chlorine contamination during ion bombardment and ions with above threshold energies during passivation, $\mathcal{S}_y$ tends to decrease with increasing ion fluence, as shown in figure 4(b). This results in decreasing $\mathcal{S}_y$ with increasing T_i, due to the increased time during which continuous etching can occur. The greatest tolerance to non-uniform ion fluxes obtained for high ion fluence occurs when $\mathcal{S}_y$ is smallest (under these conditions). This behavior is less an indication that high saturation and uniformity correlates to smaller values of $\mathcal{S}_y$ but rather it is an indication that the ALE synergy metric, as applied here, does not capture the saturation behavior.

These results indicate that in order for ALE rates to be insensitive (or less sensitive) to the uniformity of reactant fluxes, ALE surface reactions must be both self-limited and fully saturated. Ideally self-limited reactions will not provide benefits in improving uniformity if the reactions are not allowed to saturate. On the other hand, continuous etching during non-ideal ALE will also limit the benefits to uniformity. It is possible to have high values for $\mathcal{S}_y$ for under-saturated conditions, while such conditions will not improve uniformity over that of the ion fluxes. As the ion bombardment phase reaches saturation the sputtering probability of an impinging ion should decrease due to the lack of passivated sites, converging to zero for ideal ALE. This is in contrast to continuous etching where each ion should have approximately equal sputtering probability throughout the etch time. To obtain saturation, and therefore improved uniformity, an abundance of ions with low (chemical) sputtering probability is required. These ions are required for saturation, but they do not contribute to etching. In some sense, this is an inefficient use of ions. This means that in order to obtain saturation, the ALE process must intentionally over-expose the wafer to ions

compared to the continuous case. Meanwhile, the reactions must be strongly self-limited to prevent continuous etching.

Possible side-effects of this over-exposure to ions during ALE to gain uniformity include increased mask erosion and damage to stopping layers. For example, simulations of etching Si features over SiO_2 with an erodible photoresist mask (by physical sputtering) were performed for continuous etching and ALE using antenna A1. Reactant fluxes were used for two radii—1.5 cm (low fluxes) and 13.5 cm (high fluxes). The ALE cases use $T_i = 3$ s. The resulting profiles are shown in figure 5 at the time when the underlying SiO_2 is first exposed at the wafer edge (13.5 cm). The difference in etch depth from the edge to the center of the wafer is smaller for ALE processing compared to continuous etching, indicating a more uniform process. While the silicon is etched predominantly through ALE self-limited reactions, the mask erodes through non-self-limited physical sputtering. Therefore, the high ion fluence required to provide etch rate uniformity can reduce the mask selectivity and increase the fluence of ions reaching the SiO_2 etch stop layer during the over-etch. Due to the uniformity of the ALE process, only four additional ALE cycles were needed to clear the 3D '*L*' feature at the inner radius (low ion fluxes) after exposing the stopping layer at the wafer's edge (high ion fluxes). This amounted to a 16% over-etch (defined as time to completely clear the feature divided by the time to first expose the stopping layer). A 92% over-etch was required to clear the slowest etching features in the continuous etch case.

Another measure of over-etch is the total fluence of ions striking the SiO_2 stopping layer. This fluence can be directly calculated in the MCFPM by summing the ions incident onto SiO_2 material cells. Despite the reduction in over-etch as a percentage of the total etch time, during ALE etching the SiO_2 stopping layer was exposed to 33 times more ions at the edge of the wafer than at the center. For continuous etching, the stopping layer at the edge of the wafer was exposed to four times more ions than at the center.

In addition to etch depth uniformity, critical dimension (CD) uniformity is also important. In the test feature shown in figure 5, the CD is the width of the L-shaped structures. During ALE processing, the sidewalls remain passivated throughout the ion bombardment period. With there being off-axis particles in the ion angular distribution, the passivated sidewalls are exposed to ions during both continuous and ALE processing, which results in sidewall etching producing undercutting of the mask. Due to the increase in the total ion fluence during ALE processing, there is more undercutting of the mask than during continuous etching for similar etch depths. During continuous etching, re-deposition of etch products can lead to tapering of the sidewalls, the opposite of mask undercutting. This tapering can be remedied by over-etching. However, extended over-etching will eventually produce mask undercutting. When the etch times for the results shown in figure 5 were extended (over-etched) to produce features with vertical sidewalls at a radius 1.5 cm, the width of the features at a radius of 13.5 cm decreased by 50% due to mask undercutting. The undercutting and decrease in linewidth were similar between continuous etch and ALE. The amount of mask undercutting during ALE is related to T_i. As long as there are off-axis ions, longer T_i will result in more undercutting, regardless of how self-limited the surface reactions are. While ALE can improve etch depth uniformity across the wafer through its self-limited properties, it is less obvious that similar improvements in CD uniformity will automatically result.

4. Concluding remarks

ALE processing, when operated in a saturated, ion starved regime, can significantly improve the uniformity in etch rate across a wafer compared to continuous etching when the ion fluxes are not uniform. The ability of the self-limiting surface reactions to reject reactive species in over-exposed areas—either locally in a feature or globally across the wafer—can result in surface saturated reactions and uniform etch rates. This uniformity comes at the expense of over-exposing the wafer to ions (large ion fluences) compared to continuous etching. This overexposure may require careful consideration of mask and etch stop materials.

Acknowledgment

This work was supported by Lam Research Corp. the Department of Energy Office of Fusion Energy Science (DE-SC000319, DE-SC0014132) and the National Science Foundation (PHY-1500126).

ORCID iDs

Chad M Huard https://orcid.org/0000-0002-8852-6343
Steven J Lanham https://orcid.org/0000-0001-9715-4134
Mark J Kushner https://orcid.org/0000-0001-7437-8573

References

[1] Lee C G N, Kanarik K J and Gottscho R A 2014 The grand challenges of plasma etching: a manufacturing perspective *J. Phys. D: Appl. Phys.* **47** 273001
[2] Sun X-Y, Zhang Y-R, Li X-C and Wang Y-N 2015 Modulations of the plasma uniformity by low frequency sources in a large-area dual frequency inductively coupled plasma based on fluid simulations *Phys. Plasmas* **22** 53508
[3] Zhao K, Liu Y-X, Gao F, Liu G-H, Han D-M and Wang Y-N 2016 Experimental investigations of the plasma radial uniformity in single and dual frequency capacitively coupled argon discharges *Phys. Plasmas* **23** 123512
[4] Jung P G, Hoon S S, Wook C C and Young C H 2013 On the plasma uniformity of multi-electrode CCPs for large-area processing *Plasma Sources Sci. Technol.* **22** 55005
[5] Parkhe V D, Makhratchev K, Ono M and Guo Z 2015 Pixilated cooling, temperature controlled substrate support assembly *US Patent Application* 20150228513
[6] Gaff K W, Singh H, Comendant K and Vahedi V 2014 Adjusting substrate temperature to improve cd uniformity *US Patent* 8642480 B2
[7] Athavale S D and Economou D J 1996 Realization of atomic layer etching of silicon *J. Vac. Sci. Technol.* B **14** 3702
[8] Tan S, Yang W, Kanarik K J, Lill T, Vahedi V, Marks J and Gottscho R A 2015 Highly selective directional atomic

layer etching of silicon 2015 *ECS J. Solid State Sci. Technol.* **4** N5010

[9] Metzler D, Li C, Engelmann S, Bruce R L, Joseph E A and Oehrlein G S 2016 Fluorocarbon assisted atomic layer etching of SiO_2 and Si using cyclic Ar/C_4F_8 and Ar/CHF_3 plasma *J. Vac. Sci. Technol.* A **34** 01B101

[10] Sherpa S D and Ranjan A 2017 Quasi-atomic layer etching of silicon nitride *J. Vac. Sci. Technol.* A **35** 01A102

[11] Engelmann S U, Bruce R L, Nakamura M, Metzler D, Walton S G and Joseph E A 2015 Challenges of tailoring surface chemistry and plasma/surface interactions to advance atomic layer etching 2015 *ECS J. Solid State Sci. Technol.* **4** N5054

[12] Kanarik K J, Lill T, Hudson E A, Sriraman S, Tan S, Marks J, Vahedi V and Gottscho R A 2015 Overview of atomic layer etching in the semiconductor industry *J. Vac. Sci. Technol.* A **33** 20802

[13] Kanarik K J *et al* 2017 Predicting synergy in atomic layer etching (ALE) *J. Vac. Sci. Technol.* A **35** 5

[14] Tian P and Kushner M J 2017 Controlling VUV photon fluxes in pulsed inductively coupled Ar/Cl_2 plasmas and potential applications in plasma etching *Plasma Sources Sci. Technol.* **26** 24005

[15] Zhang Y, Huard C, Sriraman S, Belen J, Paterson A and Kushner M J 2017 Investigation of feature orientation and consequences of ion tilting during plasma etching with a three-dimensional feature profile simulator *J. Vac. Sci. Technol.* A **35** 21303

[16] Huard C M, Zhang Y, Sriraman S, Paterson A and Kushner M J 2017 Role of neutral transport in aspect ratio dependent plasma etching of three-dimensional features *J. Vac. Sci. Technol.* A **35** 05C301

[17] Chang J P, Arnold J, Zau G, Shin H-S and Sawin H H 1997 Kinetic study of low energy argon ion-enhanced plasma etching of polysilicon with atomic/molecular chlorine *J. Vac. Sci. Technol.* A **15** 1853